Production Engineering (2024) 18:197–206
https://doi.org/10.1007/s11740-023-01254-y

PROCESSES

Soft sensor for in-line quality control of turning processes based on non-destructive testing techniques and advanced data fusion

David Böttger[1] · Germán González[2] · Alexander Geiser[2] · Daniel Kempf[1] · Gisela Lanza[2] · Volker Schulze[2] · Bernd Wolter[1]

Received: 28 September 2023 / Accepted: 7 December 2023 / Published online: 20 January 2024

Abstract
This study describes the systematic process of training, testing, and validating a soft sensor designed for quality control of a turning process on components made of AISI 4140 steel. The soft sensor allows product quality to be predicted and unfavorable surface conditions to be identified, in particular the appearance of a phenomenon known as "White Layer", often characterized in the case of AISI 4140 steel by an ultra-fine-grained microstructure (UFG). Basis of the soft sensor is a data fusion supported by non-destructive testing techniques (NDT), particularly micromagnetic methods (3MA). A critical part of this work is to address challenges such as lift-off compensation and in-process detection using 3MA. The application of machine-learning techniques, including Principal Component Analysis (PCA) and regression analysis, is detailed. These techniques result in robust models capable of detecting the occurrence of the White Layer phenomenon while minimizing the influence of measurement setup variations and process disturbances. In addition, the study demonstrates the integration of NDT into the machining process which drives the soft sensor and allows suitable adjustments of the process parameters. The data-driven soft sensor approach demonstrates a possible In-Line control system and discusses different control theories and their respective advantages and disadvantages. This system can effectively set targeted surface conditions in real time during the turning process.

Keywords Turning process · Soft sensor · Process-model validation · White layers · 3MA · Acoustic emission

1 Introduction

When processing quenched and tempered steels a variety of surface changes can occur, with a particular focus on the formation of White Layers. These White Layers exhibit a microstructure characterized by an ultra-fine-grained appearance on the surface. In order to effectively control surface conditions throughout the machining process, a thorough understanding of the underlying mechanisms is essential. The importance of using quantitative assessment techniques and models for in-process monitoring of surface integrity is highlighted. These findings are supported by various studies.

✉ David Böttger
david.boettger@izfp.fraunhofer.de

[1] Fraunhofer Institute for Nondestructive Testing (IZFP), Campus E3 1, 66123 Saarbrücken, Germany

[2] wbk Institute of Production Science, Karlsruhe Institute of Technology (KIT), Kaiserstr. 12, 76131 Karlsruhe, Germany

Gauder et al. [1] investigated turning processes involving AISI 4140 QT steel using multivariate regression. Böttger et al. [2] introduced a soft sensor concept for predicting surface layer modifications during longitudinal turning of AISI 4140. Softs sensor is defined as Their approach included tool wear and component models based on process forces, acoustic emission, and micromagnetic material parameters. Combining one or more physical measurement principles linked with expert knowledge and mathematical models is called a soft sensor [3]. Meurer et al. [4] worked extensively on orthogonal cutting of AISI 4140 QT steel, concentrating on dynamic recrystallization and the development of White Layer. Their analytical model, based on process forces and temperature fields, facilitated the prediction of White Layer formation. Sada [5] used neural networks to predict surface conditions of mild steel after turning. Based on process parameters, their approach provided accurate forecasts for material removal rate and surface roughness. Zemzemi et al. [6] tackled the prediction of White Layer during orthogonal turning of AISI 52100 hardened steel. Their research

involved the integration of different models to anticipate cutting forces while analyzing their correlation with temperature distribution and mechanical stresses. Kuntoğlu et al. [7] studied the impact of cutting parameters on vibration and roughness when turning AISI 5140 steel. Using the response surface methodology and regression models, they optimized parameters and achieved precise predictions. Uhlmann et al. [8] studied the interaction between tool wear and machining parameters when milling AISI 4140 steel. Their work demonstrated the utility of power measurements for real-time tool wear detection and used machine learning to predict magnetic properties based on machining parameters and tool wear. Ankener and Böttger [9] performed a comprehensive micromagnetic and microstructural characterization of ferromagnetic steels under different heat treatment conditions. Their work showed the relationship between properties such as hardness, micromagnetic properties (BR, HCm, Bmax), and retained austenite content (RA). Stampfer [10, 11] discovered that lower base hardness, indicating reduced dislocation densities, is associated with higher susceptibility to predominantly mechanically induced loads compared to higher base hardness. Stampfer's analysis of AISI 4140 QT samples revealed that an increase in hardness is not always a reliable measure of surface layer modifications. This phenomenon is attributed to tempering effects caused by exceeding the tempering temperature during machining. Key findings include: X-ray analysis showed a reduction in the average FWHM (full width at half maximum) below the base material level, reflecting tempering-induced decreases in dislocation density and, consequently, hardness. Near the surface the effect is amplified by mechanically induced hardening, leading to an increase in FWHM and hardness. Significant thermal and mechanical loads can induce surface layer modifications, and their impact on hardness can be partially or fully compensated, which explains the limited sensitivity of hardness increase to process parameters compared to other tempering levels. In summary, the studies mentioned above improve our understanding of the effects of machining on steel surfaces and propose models to predict surface changes, tool wear and relevant parameters. However, there is currently a gap in the development of a model for in-situ prediction of UFG formation in AISI 4140 steel using micromagnetic.

2 Materials and methods

The starting material is low-alloy, lower-eutectoid quenched and tempered steel AISI 4140 (German standard 42CrMo4 Q+T). The chemical composition is listed in Table 1. The sample was austenitized in a vacuum furnace and quenched. The cooling rate achieved in this way was comparable to the cooling rate of conventional oil quenching. During hardening, the austenitizing temperature was 850 °C. After quenching, the specimens were annealed by holding them at different tempering temperatures of 300 °C, 450 °C and 650 °C for 60 min. As a result, high strengths are achieved with high toughness at the same time, which ensures suitability for stresses acting on the machined components. Due to the variation of the different tempering temperatures, the specimen show a different microstructure.

3 Experimental setup

As previously mentioned, the domains of ferromagnetic materials lead to the formation of nonlinear hysteresis, which forms the basis of our output parameters. Experiments were conducted on ten different samples, each of which had six different surfaces created with different cutting velocities and feed rates.

Table 2 and Fig. 1 show the cutting velocities v_c and feed rates f of the differerent section of the workpieces. Three of the ten samples were subjected to tempering temperatures of 300 °C, four to 450 °C, and three to 600 °C as shown in Table 3. The total length of a sample was 180 mm, but measurements started at 9 mm and continued until the sensor head reached 155 mm. The experiments did not start from the zero-point due to the initial need for

Table 2 Speed and feed rate for six sections of a sample

Sections of a specimen	v_c in m/min	f in mm/rev
1	100	0.05
2	100	0.15
3	100	0.30
4	300	0.05
5	300	0.15
6	300	0.30

Table 1 Chemical composition of steel AISI 4140 in weight percent

C	Si	Mn	P	S	Cr	Mo	V
0.40	0.23	0.74	0.016	0.027	1.04	0.2	0.007

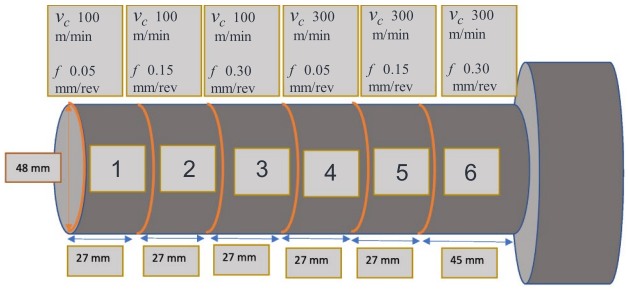

Fig. 1 Surface parameters of a sample

Table 3 Sample overview of different tempering states

Sample	Name	Tempering (°C)	Wear (µm)
1	D304	300	375
2	D305	300	40
3	D306	300	70
4	D450	450	210
5	D451	450	360
6	D452	450	0
7	D453	600	40
8	D600	600	210
9	D601	600	390
10	D602	600	70

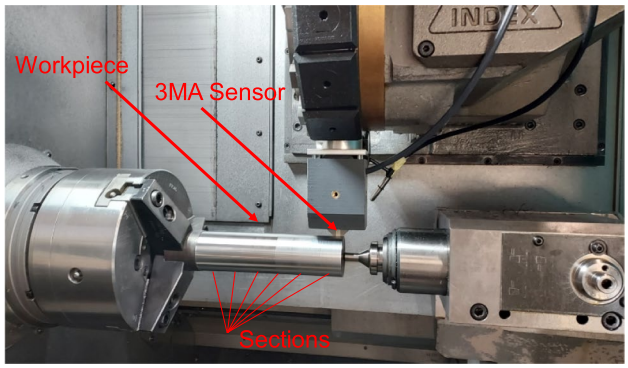

Fig. 2 Experimental setup

an area for the sensor head. The total length of the measured area was 146 mm, and the diameter of the sample was 48 mm. Abrasive tool wear on the flank face was measured after each experiment.

As a result of the turning operation, properties of the material such as surface quality, residual stress, and hardness exhibit micro-scale changes. The purpose of non-destructive material evaluation is to model these changes using sensor output values. The samples were exposed to turning operations using cutting tools with abrasive flank wear ranging from 0 to 400 µm. Later, the samples were clamped in the

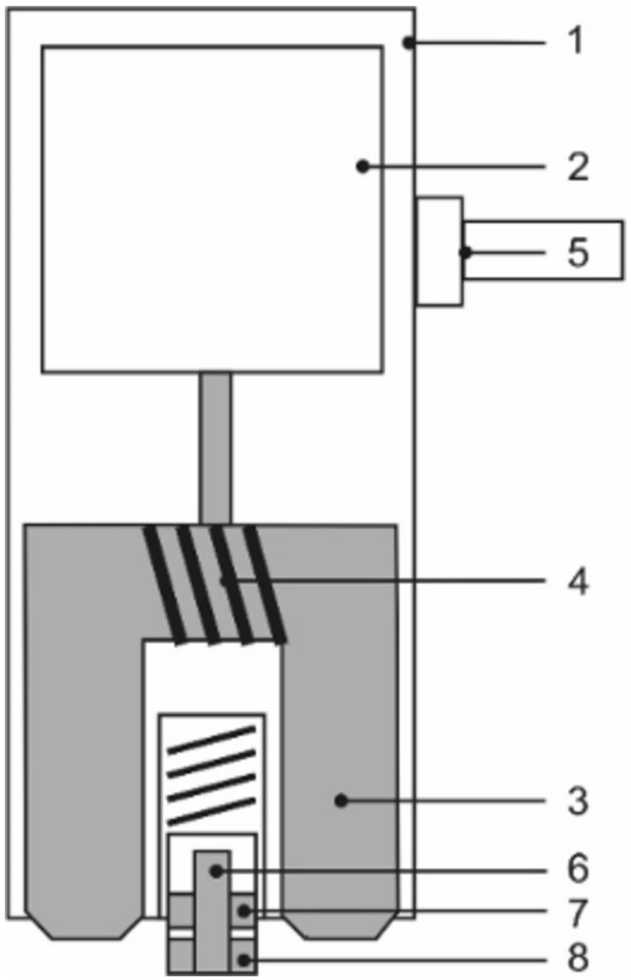

Fig. 3 Probe head with its components [12]: 1-Housing, 2-Electronic board, 3-Magnetic yoke, 4-Magnetization coils, 5-Connection cable, 6-Hall sensor, 7-Transmitter coils, and 8-Receiver coils

turning machine and measured as shown in Fig. 2. All the samples were subjected to measurements using the 3MA sensor at room temperature (24 °C) to confirm that the heating did not result in any microstructural changes.

During the experiments, variable magnetizations were utilized. The internal structure of the sensor head is shown in Fig. 3. The magnetic yoke (3) driven by the magnetization coil (2) leads to a low-frequent, high-amplitude magnetization in the sample. A Hall probe (6) and transmitter / receiver coils (7, 8) are attached in the middle between the pole shoes of the magnetic yoke. The coils are responsible for generating the high-frequent, low-amplitude magnetization for the Eddy-Current (EC) and the Incremental Permeability (IP) methods as well as for receiving the signals from EC, IP and the Barkhausen Noise (BN) method. The Hall probe is used for detecting the tangential magnetic field needed for the Harmonic Analysis (HA) method and for the control of the magnetization amplitude for all methods. Table 4 shows the

Table 4 Varying cutting parameters of the components for modelling

Shaft N°	$v_t c$ m/min	f mm/rev	Shaft N°	v_c m/min	f mm/rev
1	200	0.05	9	300	0.15
2	300	0.05	10	200	0.20
3	100	0.10	11	300	0.20
4	200	0.10	12	100	0.25
5	300	0.10	13	200	0.25
6	100	0.15	14	300	0.25
7	200	0.15	15	100	0.30
8	300	0.15	16	200	0.30

cutting parameters of the components for modelling White Layer formation based on 3MA data.

3.1 In-Line 3MA

The in-line 3MA measurement was performed with an Index G200 machine. Before the final machining and the subsequent 3MA measurement, different indexable inserts with varying wear conditions (VB) were produced by rough pre-machining during external longitudinal turning. The degree of wear was assessed by measuring the width of the wear mark VB using an optical microscope. For the samples considered here, the final machining was executed at a wear mark width of VB=38 µm. The indexable insert used was a Walter CCMT120404-RP4 WPP10S, with WPP10 denoting its suitability for high-speed machining. After a specific degree of wear, the workpiece support was removed and the individual shafts (one each for tempering temperatures of 300 °C, 450 °C, and 600 °C) were pre-machined to a diameter of 48.4 mm. The shafts were then divided into sections, each machined with different combinations of cutting parameters cutting speed v_c and feed rate f. The shafts were finally finished to a final diameter of 48 mm. After the turning process, the in-line 3MA measurement was carried out. A lift-off distance of 100 µm was chosen for positioning of the 3MA probe head. After positioning, measurements were carried out at different cutting speeds v_c and feeds f. The 3MA parameters remained constant for each combination of v_c and f. Detailed information about the specific 3MA settings can be found in Table 5.

4 Results

4.1 Investigation and compensation of positioning error disturbances

The measured data were the final stage voltage of the electromagnet V_{mag}, Maximum amplitude M_{max}, Amplitude averaged over one magnetization cycle M_{mean}, Amplitude at remanence point Mr, Maximum amplitude $umax$, Amplitude averaged over one magnetization cycle $umean$, Amplitude at remanence point ur, signal magnitudes at frequencies 4 $Mag4$.

Figure 4 shows the signal from the 3MA sensor measurements in the turning setup for a working distance variation from 100 µm to 1 mm. The obtained raw signal decreased with the increase of the measuring distance. This behaviour is observed for all the measurements. Since the distance between the 3MA sensor and the workpiece are subjected to variation due to positioning errors, variation of the workpiece diameter or to inhomogeneity on the surface roughness. The combinations of the 3MA data with the information of the measuring distance will minimize the error

Table 5 Setting parameters of 3MA measurement

	Magnetisation amplitude	High pass	Low pass	Gain	Mag Phase offset	Sharpness
	A/cm	MHz	MHz	dB	°	MPa
Harmonics	45	–	–	–	–	–
Barkhausen	60	off	1	5	32	10
		Eddy frequency kHz	Eddy amplitude dB	Eddy Gain dB	Eddy phase offset °	Mag Phase offset °
Permeability	60	150	20	15	−133.5	47
	Magnetisation amplitude A/cm	Number of frequencies –	Freq. KHz	Amp dB	Gain dB	Phase °
		1	20	25	32	0
Eddy current	15	2	50	25	18	0
		3	100	26	14	0
		4	150	30	12	0

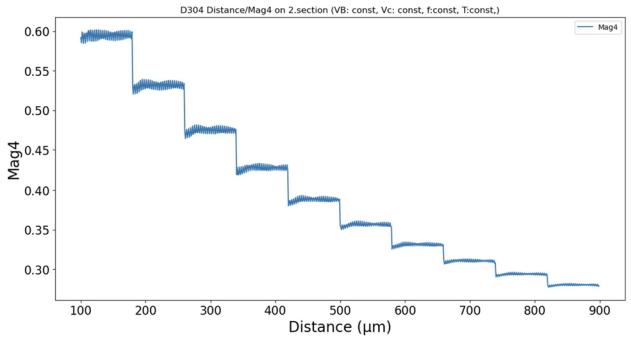

Fig. 4 Variation of signal intensity with the measuring distance

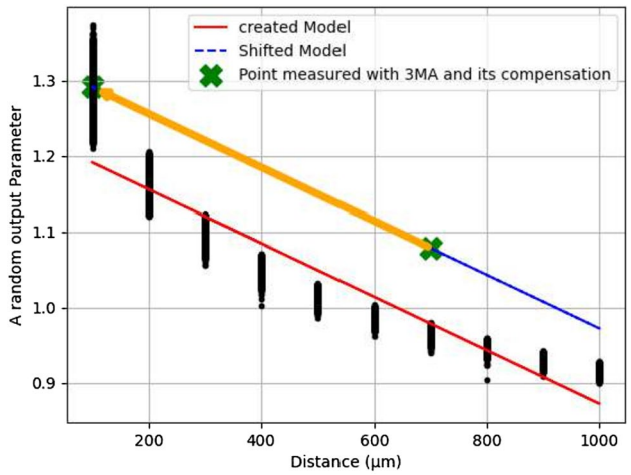

Fig. 5 Example of a Lift-off Compensation strategy using a linear regression

that comes from the Lift-off of the sensor. This strategy is depicted in Fig. 5. By means of a polynomial regression of fourth degree each of the 3MA measurements were referenced to the distance 100 µm. Figure 6 shows how this approach fit the measured values. Equation 1 describes the dependent variable y, expresses the information of the 3MA sensor depending on the measuring distance, where x is the working distance and the constants are depend on the working material and the 3MA measuring parameter.

$$y = 0.033 - 0.024 \times x + 0.01 \times x^2 - 0.008 \times x^3 + 0.0015 \times \frac{x^4}{287} \quad (1)$$

4.2 In-Line Capability of 3MA-system

Measurements were carried out on the externally longitudinally turned AISI 4140 samples, which were turned at six different machining parameter combinations (cutting speed

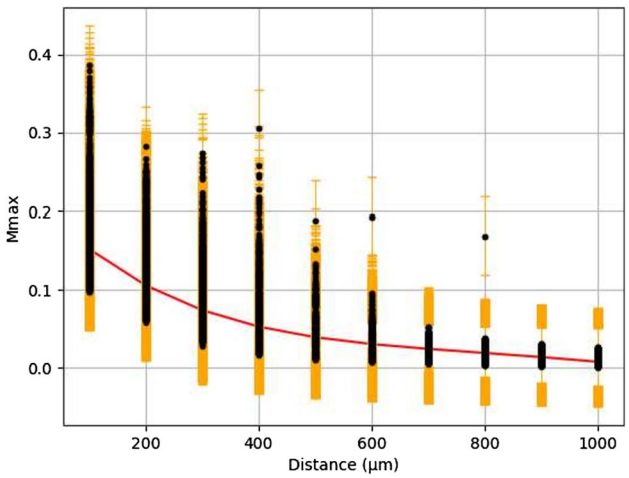

Fig. 6 4.Degree Polynomial Regression optimized with Gradient Descent

v_c and feed rate f). First, the 3MA measurement was performed at a speed of 20 min^{-1} and a feed rate of 1 mm/rev. The aim of this measurement was to create a spiral measurement of the samples by using a low rotation frequency (0.33 Hz), which is lower than the 3MA measurement frequency (6.6 Hz). Through this measurement, an orbital measurement profile was generated, in which the measured values could be assigned to an exact position on the shaft. As clearly depicted in Fig. 7, there are noticeable measurement differences among the various machining stages. The precise start and transition points between stages are marked by vertically oriented guide lines. These variations in measurement can be attributed to various factors, including mechanical and structural properties, as well as the surface topology of individual stages, each significantly influenced by the machining with different parameters. Stages 1–3 and Stages 4–6 were processed with identical cutting speeds (v_c: 100 m/min and 300 m/min respectively). However, the feed rate f varied: 0.05 mm/rev for stages 1 and 4, 0.15 mm/rev for stages 2 and 5, and 0.3 mm/rev for stages 3 and 6. The behavior of both ranges is consistent. The H_{cm} values decrease at constant cutting speed and increasing feed rate. One possible reason for this could be the heat input. At lower feed rates, there is a longer engagement time and thus a higher friction time between the tool and the shaft. Different heat inputs resulting from this could lead to varying mechanical and structural properties, such as different residual stress states. Even at higher cutting speeds at the same feed rate, the identical distance is covered between the tool and the shaft. Only the engagement time becomes shorter. Consequently, the "same" frictional energy is introduced in a shorter time. In the case of Stage 4 (v_c = 300 m/min and f = 0.05 mm/rev), the H_{cm} value significantly increases. This indicates a relatively higher heat input, causing material

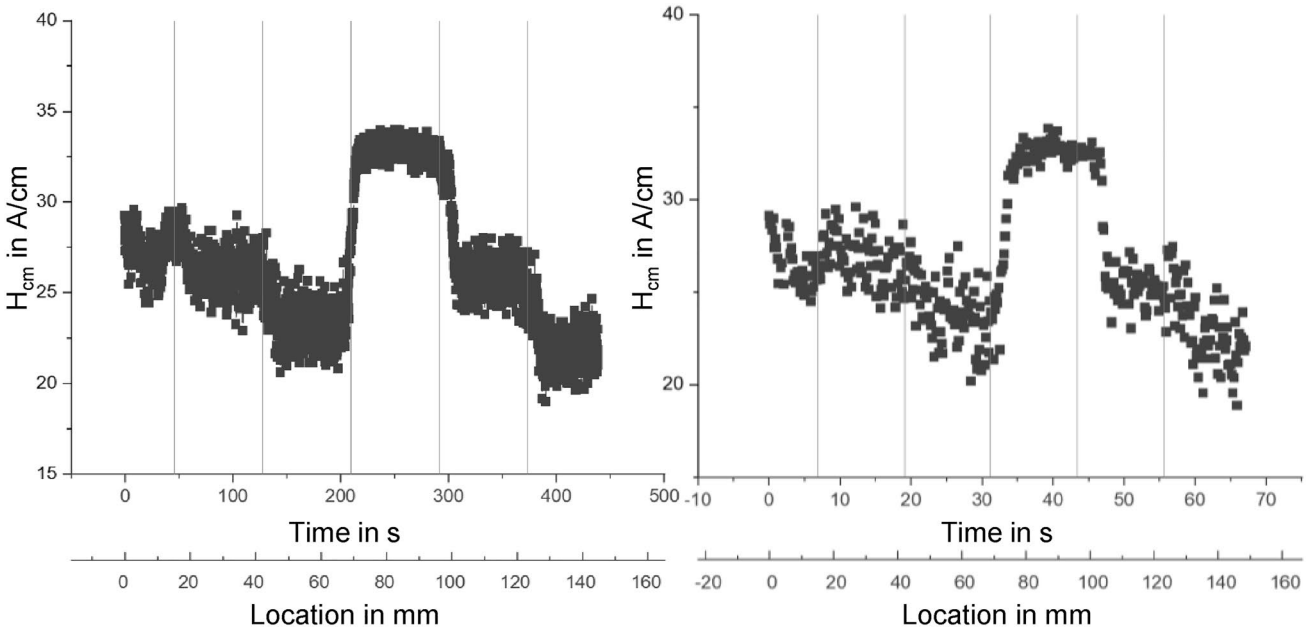

Fig. 7 3MA In-line-measurement on QT300

properties to change and resulting in notably higher H_{cm} values. In a final test, a measurement at a feed rate ($f = 0.2$ mm/rev) that was within the range of machining feed rates was performed. Here, a cutting speed of $v_c = 100$ m/min was also selected to investigate whether a 3MA in-line measurement can also be carried out under machining conditions. The results of this test are shown in Fig. 7b. It shows the same measurement data pattern as a), but with fewer measurement points. It can be concluded that the 3MA system is suitable for in-line measurement and a can serve as a possible tool for a soft sensor and the detection of White Layer.

4.3 Modelling White Layer formation based on 3MA data

The aim of modeling in this chapter is to develop a model based on the micromagnetic 3MA method. This model is intended to predict the tempering temperature. Additionally, it should enable the detection of occurring thermomechanical loads such as UFG and White Layer formation caused by different process parameters. Furthermore, the model's capability to detect extreme thermomechanical surface conditions and to identify nanocrystalline surface layers is examined. Data acquisition was performed using a pyramid-shaped specialized 3MA probe head with a small detection area. Components were measured in the post-process phase using an own at Fraunhofer IZFP developed high-speed-capable 3MA software. The experimental setup is shown in Fig. 2, with the probe head lifted by 0.1 mm during measurements. Three components at different tempering temperatures (300 °C, 450 °C, 600 °C) were used, employing the process parameters listed in Table 2. The feed rate (f) was kept constant at 0.2 mm/rev.

Measurements were conducted the the three shafts, each comprising 16 sections. The shafts rotated at a constant speed of 30 RPM. The measurement probe's lift varied slightly during the measurement due to machine tool and component vibrations, ranging from a minimum of 0.1 mm to a maximum of 0.2 mm. In the circumferential direction, 50 measurement points were taken per shaft section. Feature extraction is performed using the 3MA software, storing 40 micromagnetic measurement quantities per measurement point. In total, 96.000 data points were used for modeling in this chapter. Principle Component Analysis (PCA) from the field of multivariate statistics is used as an unsupervised method that allows grouping, interpretation and dimensional reduction of the test data. It structures higher-dimensional data sets based on the calculation of eigenvectors of the covariance matrix, resulting in the smallest possible number of meaningful principal components as a linear combination of the individual data sets. For this purpose, the variance is maximized as a measure of information content. The test data is then coloured and classified. The classes result from the three group assignments of the tests with tempering temperature T_a. The next Fig. 8 shows the respective coloured test data, (a) allows a clear separability of the annealing temperature Ta, the group 600 °C is found in quadrant I, 450 °C in quadrant II and 300 °C in quadrant III+IV.

In the next step, a classifier based on Support Vector Machine (SVM) was trained with 50-fold cross-validation

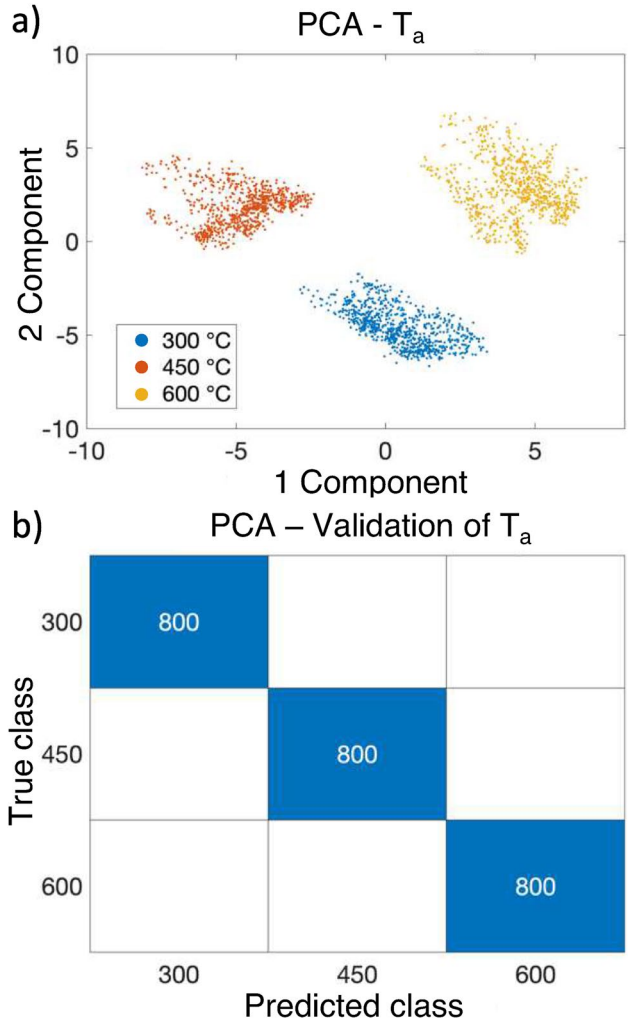

Fig. 8 1st and 2nd PCA component of tempering temperature T_a and validation via SVM confusion matrix of annealing temperature samples based on PCA

Main component	Variance
1	39,17
2	30,51
3	10,08
4	7,5
5	4,49
6	2,26
7	1,49

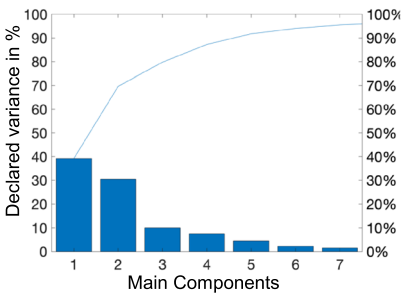

Fig. 9 Pareto diagram with variance of principal component analysis

for the three group memberships, resulting in three tempering conditions of 800 observations with 50 test sets of a training size of 2352 and a test size of 48. Figure 8b shows the confusion matrix of the detected tempering temperature. It can be observed that the predicted classes of annealing temperatures are reliably detected with 800 observations each showing a prediction rate of 100%. The annealing temperature thus has a systematic influence. The corresponding Pareto diagram is shown in Fig. 9.

This illustrates the variance contributed by each principal component and its cumulative distribution, up to a threshold of 95%. It can be seen that components 1 and 2 explain 69.68% of the variance and seven components are necessary for a 95% variance. By means of PCA, a dimensional reduction of the micromagnetic test data can thus be carried out, where seven components explain already 95% of the original information. During our investigations, a new tool with no tool wear and therefore small thermomechanical loads and small or medium mechanical loads does not lead to the formation of nanocrystalline layers. Medium tool wear ($VB = 130\ \mu$m) leads to barely measurable ultrafine-grained (UFG) structures, but instead, high tool wear ($VB = 420\ \mu$m) in combination with large mechanical loads leads to large thermal loads and thus favors the formation of nanocrystalline layers. The UFG that occurred in all samples had a thickness variation in the radial circumferential direction. Figure 10 shows the 3MA test data recorded at selected temper and UFG conditions, plotted as test data in the PCA model for the 1st and 2nd principal components.

A formation of UFG ≤ 10 µm occurred for 450 °C samples, VB = 130 µm at medium mechanical load. As seen in Fig. 10a, the data arrange themselves in a wide range from overlapping the training group 450 °C in the II quadrant to beyond the training group 300 °C in the III and IV quadrant, with values of – 8 for the 1st component and 8 for the 2nd component. This indicates an increase in thermal influence due to tool wear despite medium mechanical load, as the test data extend beyond the 300 °C training group. It could be proven that a hardening of the surface layer occurred with an increase in hardness to 700–800 HV similar to the 300 °C training group.

In Fig. 10b, a formation of UFG ≥ 10 µm for 300 °C, VB = 420 µm due to high mechanical load is shown and as expected, the test data shift even more to the IV quadrant and show no overlapping with the original training group. Therefore, a distance quantity x is defined on the basis of the 2nd component to give an estimation of the distance to the edge of the training group. At the intercept – 9 is defined as the limit, where if the value has fallen below, a formation of UFG has taken place. This value is drawn as a dashed line in red, the dashed line in blue at axis intercept – 7 is intended to serve as a safety limit for further control process aspects. The limit is far undercut and shows values up to – 17.

To avoid occurring UFG, the hardness increase in the surface layer and the respective tempering temperature of the base material are of interest. Large increases in hardness only occur in AISI 4140 QT 300 due to a combination

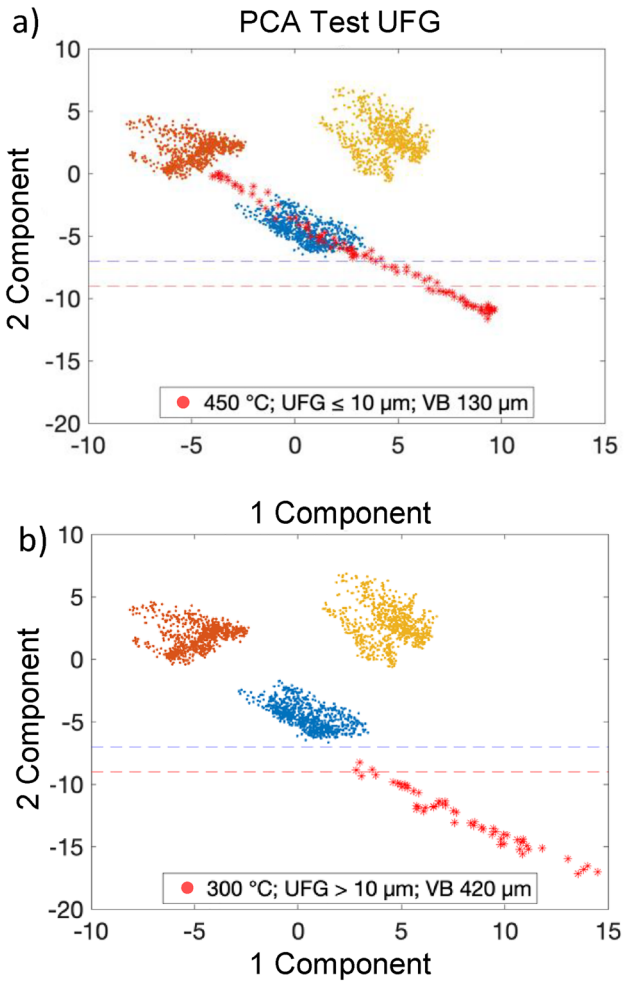

Fig. 10 3MA test data as test data in the PCA model with formation of UFG ≤ 10 µm for QT450, VB = 130 µm at high mechanical load and formation of UFG ≥ 10 µm for QT300, VB = 420 µm, high mechanical load. The specifications of the UFG in µm refer to the depth effect

of high thermal and mechanical loads, which favors the formation of UFG. This leads to the qualitative correlation between process variables and the hardness increase ΔHV. Based on the findings mentioned before, a parameter UFG_{3MA} is defined. It contains a case distinction based on the mentioned limit of the 2_{nd} component based on 3MA data. By means of this, a percentage ratio is formed between -7 and -9, which ranges from 0 % to 100 %. The parameter UFG_{3MA} is defined in Eq. 2:

$$UFG_{3MA}(x) = \begin{cases} 0 & , x > -7 \\ -0.5 \times x - 3.5 & , -7 \geq x > -9 \\ 1 & , x \leq -9 \end{cases} \quad (2)$$

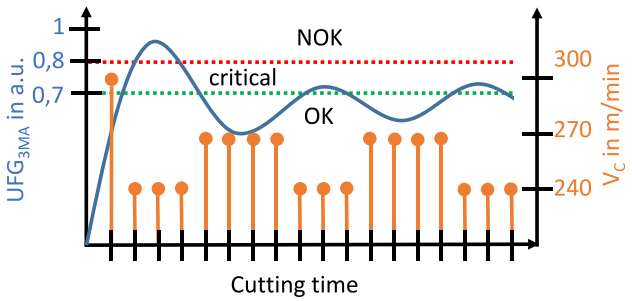

Fig. 11 Potential surface states adjustment based on UFG_{3MA} by adjusting the cutting speed between consecutive cuts

It should be noted that no UFG have been formed for values between $0 < UFG_{3MA} < 1$. At $UFG_{3MA} > 1$, a formation of UFG has occurred.

4.4 Cut-to-cut controlled surface states adjustment

Building upon the previously discussed variable, there are opportunities for effective process control and regulation. In the context of optimizing machining productivity, the goal is to achieve a high cutting speed and a significant high feed rate. Figure 11 outlines a potential process control method that involves adjusting the cutting speed between consecutive cuts.

When the value surpasses the unfavorable range (NOK) with $UFG_{3MA} > 0.8$, the control process may commence. Upon reentering the favorable range (OK) with $UFG_{3MA} < 0.7$, an attempt would be made to fine-tune the process parameters, While prioritizing the attainment of high production efficiency. The aim is to regulate cutting speed and therefore the UFG_{3MA} parameter within the critical range or in proximity to it, avoiding any transition into the unfavorable range.

If the value exceeds the unfavorable range (NOK) with $UFG_{3MA} > 0.8$, the control process can begin. Here v_c is reduced by factor 0.8 (240 m/min). Subsequently UFG_{3MA} settles over the critical- towards the favorable range. Upon re-entry into the favorable range (OK) with $UFG_{3MA} < 0.7$, an attempt is made to fine-tune the process parameters, aiming for high production efficiency. Here, v_c is increased again (270 m/min). For further cuts, v_c oscillates between 240 and 270 m/min to avoid a transition into the unfavorable range. Thus, the objective can be to keep the parameter UFG_{3MA}, which signals a formation of fine-grained microstructure, within or close to the critical range to allow a high production efficiency.

5 Conclusion

A key finding of the study presented here is the need to address lift-off compensation and in-process detection of fine-grained microstructures known as White Layers on AISI4140 through newly developed training, testing and validation methods based on 3MA data. This approach enables the prediction of product quality and the identification of undesirable surface conditions during turning processes. The development of the UFG_{3MA} parameter plays a central role in the creation of a soft sensor. In summary, the control of the process is initiated when the value surpasses the unfavorable range (NOK) leading to adjustments in process parameters aimed at maintaining the UFG_{3MA} parameter within or near the critical range, thereby facilitating high production efficiency. Different control models suited for establishing a robust closed-loop control system aimed at managing adverse surface conditions during the turning production process in real-time in the next section.

6 Outlook: In-Line process control for surface conditioning

Starting from the control system where the machine parameters are readjusted between the individual cuts, an online control system for the turning process is to be implemented in the future. Building on the study of the 3MA variables and their influence on the characterisation of machining processes, this section provides a comprehensive discourse on quality control strategies. The primary goal is to proactively control and prevent the formation of UFG while archiving the maximum material removal rate and therefore maintaining the lowest possible production times. In order to do so a soft sensor will be developed with input of 3MA and output process control variables. Process control implementation necessitates both hardware and software to manipulate process parameters. In the case of CNC turning machines, the goal is to link the feed rate and cutting velocity overrides with NC code parameters and externally regulate them through an industrial PC. Converting discrepancies in target values to control variables involves the application of control design principles. For this, the three control theories, PID controller, Model Predictive Controller (MPC) and Reinforcement Learning (RL) were compared. The widely used PID controller is effective for simple linear systems but falls short in handling complex tasks and non-linear systems [13]. Despite its adaptability, limitations arise in addressing uncertainties and time delays [14]. MPC, formulated as an optimization problem, proves promising for complex tasks by considering multiple objectives and constraints [15]. While requiring an accurate model and careful modeling, MPC's theoretical applicability to various systems makes it a viable choice for cutting process control [16]. RL, with adaptive learning properties, excels in handling complex dynamics but faces challenges in setting hyperparameters and requiring substantial data for optimization [17–19]. MPC emerges as the most suitable option for precise control of cutting processes due to its applicability to demanding and complex tasks [20]. It allows simultaneous optimization of multiple quality measures and simplifies problem formulation through mathematical objectives and constraints [21].

Acknowledgements The authors gratefully acknowledge the financial support of the German Research Foundation, Deutsche Forschungsgemeinschaft (DFG) within the research priority program SPP2086 "Surface Conditioning in machining" SCHU 1010/65-2, LA 2351/46-2 and WO 903/4-2.

Funding Open Access funding enabled and organized by Projekt DEAL.

Declarations

Conflict of interest The authors declare that they have no conflict of interest.

References

1. Gauder D, Biehler M, Gölz J, Stampfer B, Böttger D, Häfner B, Wolter B, Schulze V, Lanza G (2021) Development of a methodical approach for uncertainty quantification and meta-modeling of surface hardness in white layers of longitudinal turned aisi4140 surfaces. J Name. https://doi.org/10.1515/teme-2021-0037
2. Böttge D et al (2020) Concept for soft sensor structure for turning processes of aisi4140. tm-Technisches Messen 88(11):744–750. https://doi.org/10.1515/teme-2020-0054. (**DFG priority program 2086, project: In-process soft sensor for surface-conditioning during longitudinal turning of AISI4140**)
3. Schulze V, Zanger F, Stampfer B, Seewig J, Uebel J, Zabel A, Wolter B, Böttger D (2020) Surface conditioning in machining processes: glossary of the dfg priority programme 2086. tm-Technisches Messen 87(11):661–673. https://doi.org/10.1515/teme-2020-0044

4. Meurer M, Bergs T, Schraknepper D (2023) Investigation of the mechanical workpiece loading during orthogonal cutting aisi 4140 by means of digital image correlation. Proc CIRP. https://doi.org/10.1016/j.procir.2023.06.088
5. Sada SO (2021) Improving the predictive accuracy of artificial neural network (ann) approach in a mild steel turning operation. Int J Adv Manuf Technol 112(9–10):2389–2398
6. Zemzemi F et al (2021) Analytical multi-physics model of microstructure changes in hard turning of aisi 52100 steel: prediction of thicknesses of white and dark layers. Int J Adv Manuf Technol 112(9–10):2755–2771
7. Kuntoğlu M et al (2020) Modeling of cutting parameters and tool geometry for multi-criteria optimization of surface roughness and vibration via response surface methodology in turning of aisi 5140 steel. Materials 13(19):4242
8. Uhlmann E et al (2021) Machine learning of surface layer property prediction for milling operations. J Manuf Mater Process 5:104
9. Ankener W et al (2021) Micromagnetic and microstructural characterization of ferromagnetic steels in different heat treatment conditions. J Manuf Mater Process 5:104. https://doi.org/10.3390/jmmp5010004
10. Stampfer B, Bachmann J, Gauder D, Böttger D, Gerstenmeyer M, Lanza G, Wolter B, Schulze V (2022) Modeling of surface hardening and roughness induced by turning aisi 4140 qt under different machining conditions. In: Procedia CIRP 87 5th CIRP CSO 2020. https://doi.org/10.1016/j.procir.2022.03.050
11. Stampfer B. Entwicklung Eines Multimodalen Prozessmodells zur Oberflächenkonditionierung Beim Außenlängsdrehen Von 42CrMo4. https://doi.org/10.5445/IR/1000156133
12. Wolter B, Gabi Y, Conrad C (2019) Nondestructive testing with 3ma-an overview of principles and applications. Appl Sci 9:1068. https://doi.org/10.3390/app9061068
13. Najariyan M, Zhao Y (2021) Granular fuzzy pid controller. Expert Syst Appl 167:114182
14. Atherton DP, Majhi S (1999) Limitations of pid controllers. In: Proceedings of the 1999 American Control Conference (Cat. No. 99CH36251), vol. 6, pp 3843–3847. IEEE
15. Schwenzer M, Ay M, Bergs T, Abel D (2021) Review on model predictive control: an engineering perspective. Int J Adv Manuf Technol 117(5–6):1327–1349
16. Morari M, Lee JH (1999) Model predictive control: past, present and future. Comput Chem Eng 23(4–5):667–682
17. Bellman R (1957) Dynamic programming. Princeton University Press
18. Lee JH, Kim HJ (2022) Reinforcement learning for robotic flow shop scheduling with processing time variations. Int J Prod Res 60(7):2346–2368
19. Panzer M, Bender B (2022) Deep reinforcement learning in production systems: a systematic literature review. Int J Prod Res 60(13):4316–4341
20. Huang Y, Fard SM, Khazraee M, Wang H, Khajepour A (2017) An adaptive model predictive controller for a novel battery-powered anti-idling system of service vehicles. Energy 127:318–327
21. Sekhar R, Singh TP, Shah P (2022) Machine learning based predictive modeling and control of surface roughness generation while machining micro boron carbide and carbon nanotube particle reinforced al-mg matrix composites. Part Sci Technol 40(3):355–372